Ferroelectrcity and Large Piezoelectric Response of AlN/ScN superlattice

Mohammad Noor-A-Alam, Oskar Z. Olszewski and Michael Nolan

*Tyndall National Institute, Lee Maltings, Dyke Parade, University College Cork, Cork, T12 R5CP, Ireland, *Corresponding author: Michael Nolan (michael.nolan@tyndall.ie)*

E-mail:

Abstract

Based on density functional theory, we investigate the ferroelectric and piezoelectric properties of the AlN/ScN superlattice, consists of ScN and AlN buckled monolayers alternating along crystallographic c-direction. We find that the polar wurtzite (w-ScAlN) structure is mechanically and dynamically stable, and is more stable than the nonpolar hexagonal flat configuration. We show that ferroelectric polarization switching can be possible for epitaxially tensile strained superlattice. Due to the elastic constant C_{33} softening along with an increase in e_{33}, the piezoelectric coefficient d_{33} of the superlattice is doubled compared to pure w-AlN. The combined enhancement of Born effective charges (Z_{33}) and the sensitivity of the atomic co-ordinates to external strain ($\frac{\partial u_3}{\partial \eta_3}$) is the origin of large piezoelectric constant e_{33}. Moreover, we show that epitaxial biaxial tensile strain significantly enhances the piezo-response, so that d_{33} becomes seven times larger than that of w-AlN at 4% strain. The tensile strain results in a huge enhancement in e_{33} by increasing Z_{33} and $\frac{\partial u_3}{\partial \eta_3}$, which boosts the piezoelectric coefficient. As short-period superlattice growth and epitaxial strain are already experimentally demonstrated in wurtzite nitrides, our results show a new more controlled approach

to significantly enhance and tune the piezoelectric response of w-AlN materials with additional possibility of ferroelectricity.

Introduction

Over the past two decades, piezoelectric microelectromechanical systems (MEMS) have become attractive in multiple applications, including high frequency and temperature-stable resonators that have significantly miniaturised cell phones, piezoelectric sensors and energy harvesting devices. Suitable non-toxic (lead-free) and cheap piezoelectrics with a high piezoelectric response are required for these devices. In this respect, environment friendly lead-free wurtzite AlN (w-AlN) has already demonstrated significant potential for realizing more complex sensing and mobile communication systems mainly due to the compatibility of AlN devices with complementary metal oxide semiconductor (CMOS). A high Curie temperature, low acoustic and dielectric losses, high acoustic wave velocity, and compatibility with established silicon manufacturing process make AlN a perfect candidate for various MEMS/NEMS devices[1–5]. High performance RF filters made of AlN based resonators also show great promise for mobile communication systems[1,6–8]. However, the low electromechanical coupling coefficient, which is closely related to the piezoelectric coefficients, is the main disadvantage of pure w-AlN. Therefore, enhancement of this coupling in AlN based materials in a reliable and tunable way as well as atomistic understanding of the mechanism behind it are the key challenges for both academia and industry[1,9–12].

Promisingly, recent experiments have demonstrated a significant enhancement for piezo-response in doped w-AlN[9,11–13]. For example, a $Sc_{0.5}Al_{0.5}N$ alloy shows a huge (about 400%) increase of the piezoelectric constant d_{33} when compared to pure w-AlN[14]. As the Sc concentration increases, the piezoelectric constant e_{33} increases because of a large increase in the sensitivity of the internal coordinates of the atoms to strain[14,15]. Such a significant increase in e_{33} along with profound softening of the elastic constant C_{33}, which arises because of the

2

energy landscape flattening as a result of a competition between the hexagonal and the parent wurtzite phases, drives a tremendous increase in d_{33}[14]. However, the major difficulties with these alloys that prevent their widespread use are (i) the high Sc-doping concentration leads to a phase transition that completely suppresses the piezoelectricity, although the significant enhancement in piezoelectricity is only observed at high Sc concentrations, which are near the phase transition[9] and (ii) the material properties largely depend on the configurations of the dopants[16], which are formed essentially randomly during the sputtering process. It is therefore hard to control the reliability and reproducibility required for device performance. In this regard, an ordered structure such as a superlattice with enhanced piezo-response is explored in this paper as an alternative approach to realize the fabrication of stable ScAlN alloys with a high concentration of Sc.

Over the last few decades, the superlattices of short-period group-III nitrides have been studied mainly for their optical properties[17−25]. The fabrication of 1:1 wurtzite group-III nitride heterostructures with long range ordering by metalorganic vapor phase epitaxy (MOVPE) has demonstrated a new way to design nitrides with desired properties[18]. Recently binary short-period superlattice of InN/GaN with a monolayer thick InN has been fabricated using molecular beam epitaxy (MBE)[26−28]. Also, GaN atomic layers as thin as two atomic layers isolated by AlN barriers have grown by MOVPE[29]. More recently plasma assisted MBE has been successfully used to grow a monolayer of GaN sandwiched between AlN barriers[30]. Wurtzite InGaN nanowires with a 1:1 periodic atomic-level chemical ordering along the c-direction has been demonstrated[31]. Films consisting of one layer each of GaN and ScN have also been grown[32]. Interestingly, spontaneously formed superlattice structures of nitrides are also quite common[33−35].Piezoelectric properties of such 1:1 superlattices have also been studied theoretically[19,20,36], although there is at present no experimental information. Theoretically, it has been also shown that hydrostatic pressure in these superlattices can significantly enhance the piezoelectric response[19,20].Moreover, the atomistic mechanisms behind the piezoelectric enhancement and dynamical or mechanical stability
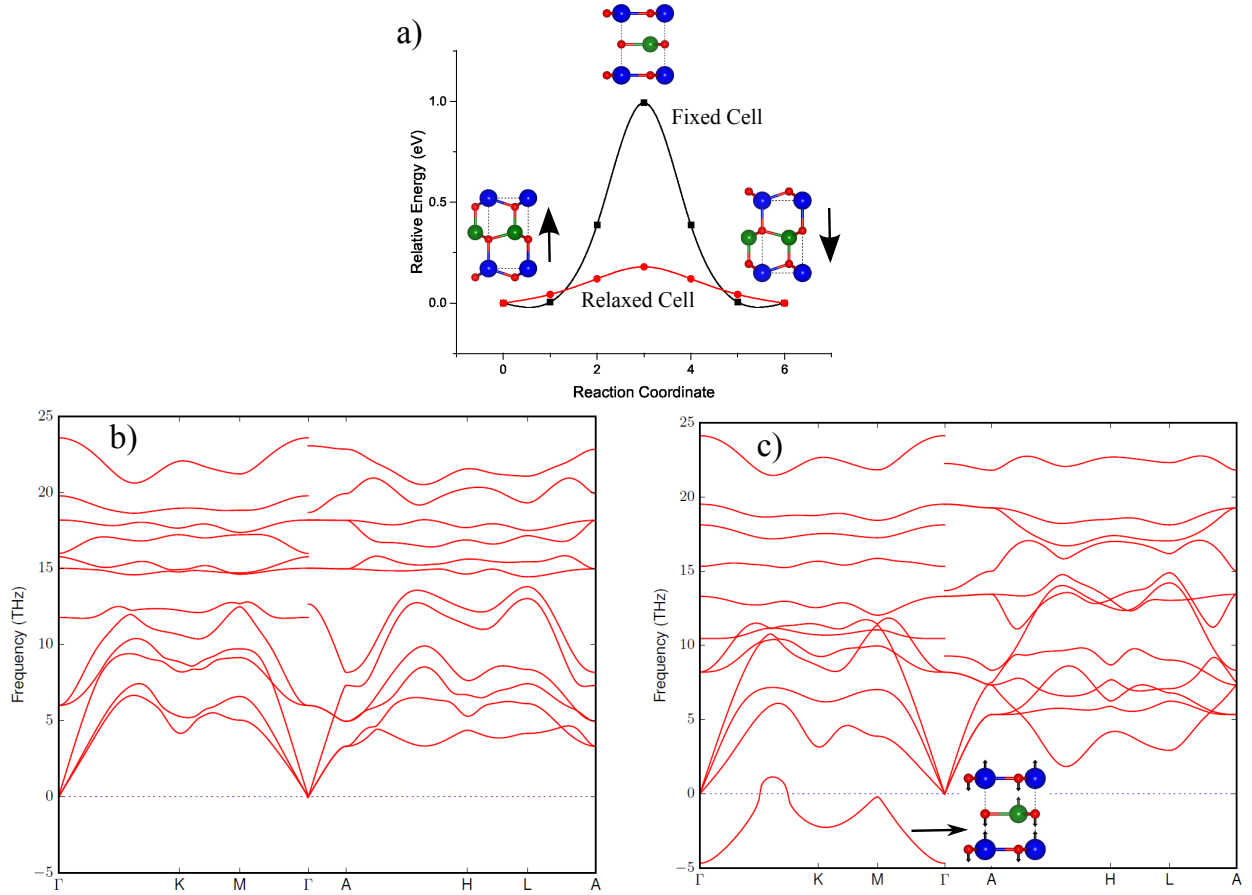
Figure 1: (a) Energy barrier for polarization switching by flatting of Al(Sc)-N plane. Black curve shows the energy barrier when the unit cell is fixed to polar configuration during the switching, while red curve shows the energy barrier when the unit cell is relaxed using SS-NEB method. (b) and (c) Phonon band structure of w-ScAlN and h-ScAlN, respectively. Inset in (c) shows the atomic displacement of the imaginary mode. The discontinuity in the phonon dispersion at Γ is originated from the non-analytical term added to dynamical matrix to treat the long-range Coulomb interaction in the polar materials.

of the ScAlN superlatticeare not yet clearly understood. In addition, a controlled way to enhance and tune the piezoelectric properties is desired for practical device applications. To our best knowledge, possibility of ferroelectricity in ScAlN superlattices has also remained unexplored.

In this study, we investigate the origin of the enhanced piezoelectric constants in a 1:1 ScN-AlN superlattice. We show that although wurtzite nitrides are polar materials with large polarization switching barriers that hinder applications in ferroelectric devices, ferroelectric polarization switching can be realized in the superlattice, which adds new functionalities to wurtzite-structured nitrides. Ferroelectricity in highly Sc doped w-AlN was recently predicted[25], although the phase stability problem at high Sc concentration still persists[9]. Furthermore, we propose that epitaxial biaxal tensile strain in ScAlN can reduce the polarization switching barrier, and increase d_{33} by a factor of seven compared to pure w-AlN. The applied strain leads the structure closer to a phase transition from wurtzite-like to graphitic hexagonal structure. A similar enhancement in piezoelectric properties is well-known for ferroelectric perovskites near to the phase-transition region[37,38]. We also mentioned that epitaxial strain has been intensively studied both theoretically and experimentally for inducing ferroelectricity in paraelectric perovskites[39,40] and rock-salt non-ferroelectric materials[41].

Computational Details

Our first-principles calculations are performed in the framework of spin-polarized density functional theory using projector augmented wave (PAW) potentials to describe the core electrons and the generalized gradient approximation (GGA) of Perdew, Burke, and Ernzerhof (PBE) for exchange and correlation as implemented in the Vienna Ab initio Simulation Package (VASP)[42–44] based on a plane-wave basis set. A cutoff energy of 500 eV for the plane-wave expansion is used in all calculations and all structures are fully relaxed until the Hellmann-Feynman forces on all the atoms are less than 10^{-3} eV/Å. The lattice parameters

and internal coordinates of the structures are fully relaxed to achieve the lowest energy configurations using conjugate gradient algorithm. Geometry optimization of ScAlN is carried out employing the conjugated gradient technique and the convergence for the total energy is set as 10^{-7} eV. The Brillouin zone is sampled with a Γ -centered k -point mesh of $15 \times 15 \times 15$ for geometry optimizations, while a denser grid of $25 \times 25 \times 25$ is used for electric polarization calculations. Density functional perturbation theory (DFPT) is used to calculate elastic (C_{ij}), Born effective charges (Z^*_{ij})and piezoelectric (e_{ij}) tensors. We compare the structural parameters and spontaneous polarization obtained from the local density approximation (LDA), GGA, and Heyd-Scuseria-Ernzerhof (HSE06) exchange-correlation functionals, and find that three functionals produce reasonably close values (see Supplementary Information). All the results in this paper are obtained from GGA calculations. Phonon bandstructures are calculated from $3 \times 3 \times 3$ supercell of the primitive cell using DFPT employing phonopy code[45]. The nudged elastic band method (NEB)[46] with five images is employed to calculate the polarization switching energy barrier. Recently developed solid-state NEB (SSNEB)[47] with five images has also been used to calculate the barrier as this method allows relaxation of atomic and cell degrees of freedom for each image, whereas NEB only allows atomic relaxation for each image keeping the lattice parameters same for all the images. The images are relaxed until the maximum force per atom was no more than 0.05 eV/Å.

Results and discussion

The ordered wurtzite-like ScAlN 1:1 superlattice (w-ScAlN), shown in Fig 1, consists of one layer of buckled ScN and buckled AlN alternating along the c-direction. The calculated lattice constant ($a=b$) for the w-ScAlN superlatice is 3.33 Å, which is larger than that of pure w-AlN (3.13 Å) but smaller than that of h-ScN (3.69 Å). The c/a ratio of the superlattice is 1.56, which is slightly lower than that of pure w-AlN (1.60). Two different internal parameters u, a dimensionless parameter that determines the position of the atoms
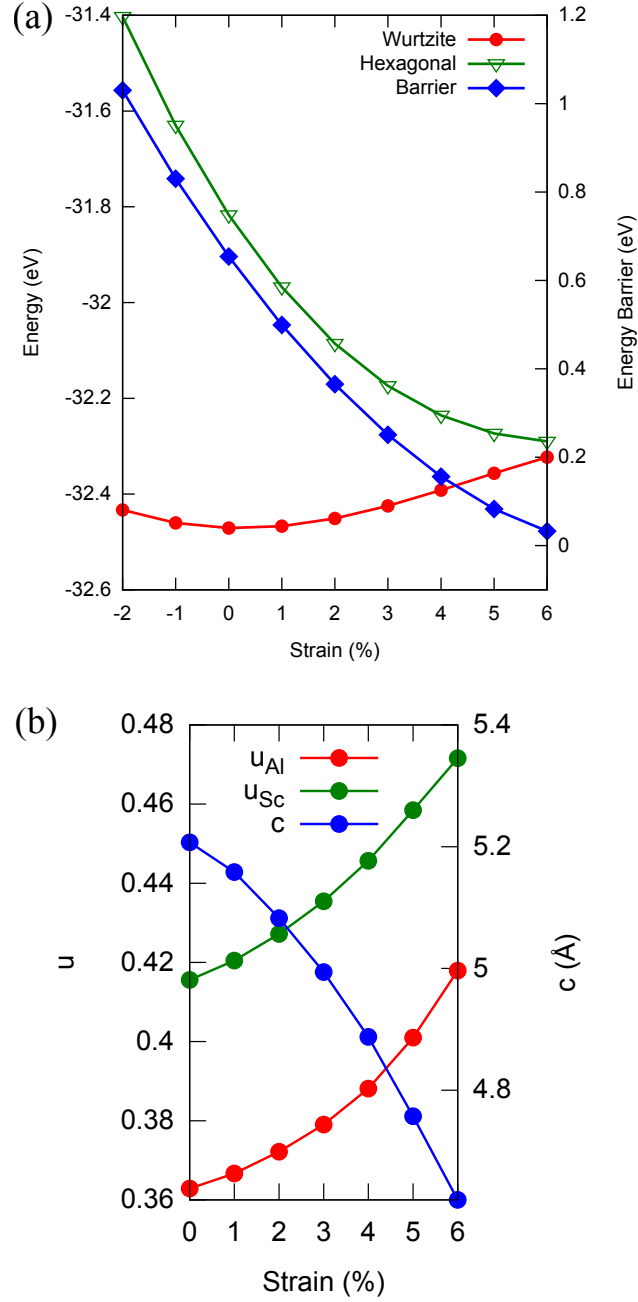
Figure 2: (a) Total energy per formula unit of w-ScAlN and h-ScAlN with epitaxial strain. The energy barrier is defined as the energy difference between the wurtzite and the hexagonal phase of ScAlN superlattice, where h-ScAlN has the wurtzite's in-plane lattice parameter. (b) Change of internal parameters (u_{Sc} and u_{Al}) and lattice parameter c with epitaxial strain.

in the unit cell, are calculated (u_{Sc} = 0.416 for Sc and u_{Al}= 0.363 for Al). The u parameter of pure w-AlN (u = 0.382) is in between these two values. The w-ScAlN structure is 0.16 eV lower in energy with respect to the hexagonal (h-ScAlN) structure with u = 0.50, where each flat ScN and flat AlN layer repeats along the c-direction. In fact, w-ScAlN is also lower in energy with respect to 4H- and 6H-type configurations (structures are shown in Fig. S1 in Supplementary Information). The formation energy per atom (E_f) is defined as $E_f = (E_{w-ScAlN} - E_{bulk-Sc} - E_{bulk-Al} - E_{N_2})/N$, where $E_{w-ScAlN}$ is the energy per atom of w-ScAlN, $E_{bulk-Sc}$and $E_{bulk-Al}$ are energy per atom of bulk Al (space group: Fm3m) and bulk Sc (space group: P63/mmc), respectively, E_{N_2} is the energy of N_2 molecule and N is the total number of atoms in the primitive unit cell (4 atoms). In high temperature growth techniques, N_2 molecule rather than solid N_2 is a reasonable energy reference for formation energy. The negative formation energy of w-ScAlN (-1.44 eV/atom, which is close to the formation energy of w-GaN[48]) indicates its stability with respect to bulk Al, bulk Sc and N_2 molecule. As the w-ScAlN superlattice is a new structure, its mechanical or elastic stability is checked according to the criteria for a hexagonal crystal structure[49]: C_{11}> C_{12}, $2C_{13}^2$< $C_{33}(C_{11}+C_{12})$, C_{44} > 0, C_{66} >0. Considering the five independent elastic constants that we obtain, namely C_{11}= 264.72 GPa, C_{12}= 115.02 GPa, C_{13}= 122.82 GPa, C_{33}= 202.21 GPa, and C_{44}= 67.47 GPa, C_{66}= $(C_{11}$-$C_{12})/2$, it can be concluded that the ScAlN superlattice is mechanically stable.

To confirm the dynamical stability of w-ScAlN, the phonon dispersion is also calculated (shown in Fig. 1). The absence of any imaginary modes in the phonon bandstructure confirms that the structure is stable or at least structurally metastable. On the other hand, the hexagonal phase shows an imaginary optical phonon mode that has the lowest imaginary frequency (i4.58 THz) at the center of the Brillouin zone (Γ-point). This soft mode represents a set of atomic displacements where Al or Sc and N atoms are moving in opposite directions along the c-axis. The lowest imaginary phonon mode at Γ guarantees an identical atomic displacement pattern in each unit cell, which results in a ferroelectric polarization (shown in

Fig. 1(c)).

In a real wurtzite crystal, a spontaneous polarization along the c-direction is a consequence of the deviation of the c/a ratio (as well as the u parameter) from the ideal value of 1.633 (u=0.375). The c/a ratio for both w-AlN and w-ScAlN is lower than the ideal value, resulting a spontaneous polarization along c-direction. Using Born effective charges (Z_{33}^*) and atomic displacement ($\triangle u_{k,3}$) along the c-direction with respect to non-polar hexagonal configuration, we calculate spontaneous polarization along the c-direction (P_3) using the following expression[50]:

$$P_3 = \frac{e}{\Omega} \sum_k \overline{Z_{k,33}^*} \triangle u_{k,3} \tag{1}$$

where k represents the different ions in the unit cell. As the value of Z_{33}^* of each ion changes during the transition (i.e. polarization switching) from the wurtzite to the hexagonal configuration, we take the mean value ($\overline{Z_{33}^*}$). This formula is commonly used for ferroelectric perovskites[51]. Our calculated P_3 for w-AlN is 1.30 C/m^2, which is quite comparable with recently corrected value (1.35 C/m^2) considering non-polar hexagonal configuration as the paraelectric reference[50]. The P_3 for w-ScAlN directing from the N layer to the Al/Sc layer along the c-direction is 1.12 C/m^2 , which is slightly smaller than that of w-AlN. Note that w-ScAlN possess a spontaneous polarization about four times larger than that of BaTiO$_3$ (ca. 0.27 C/m^2)[52], and even slightly higher than that of well known ferroelectric PbTiO$_3$ (0.81 C/m^2)[53]. Hence, the possibility of polarization switching could make w-ScAlN a promising candidate for ferroelectricity.

As the energy difference between wurtzite and hexagonal phases for AlN is high (ca. 0.56 eV/unit cell), ferroelectric switching of this spontaneous polarization may not be practical. Additionally, a large structural change during the switching from the wurtzite to the hexagonal structure, in which the axial lattice parameters (a and b) lengthen by 6.7% and the c parameter decreases by 17.94% , hinders ferroelectric switching in bulk w-AlN. However, opening the possibility of ferroelctricity, the polarization switching barrier (0.16 eV/unit

cell) of the w-ScAlN superlattice (obtained from SSNEB calculation as shown in Fig. 1(a)) is significantly lower than that of w-AlN. The underlying mechanism for the decrease in thee energy difference is due to the fact that there exists a metastable hexagonal ScN phase, although the ground state crystal structure of ScN is rocksalt cubic, and its wurtzite phase is unstable[54,55]. The presence of such metastable hexagonal ScN phase in ScGaN alloy grown by molecular beam epitaxy has also been experimentally confirmed[56,57]. In fact, the internal parameter $u_{Sc} = 0.416$ in ScAlN is closer to the value of 0.5 for the hexagonal phase than the wurtzite phase. Note that similar value of u_{Sc} is also observed for the Sc atoms in Sc doped w-AlN, where the high concentration of Sc drives the wurtzite to hexagonal phase transition by increasing u_{Sc} monotonically and consequently ferroelectricity is also predicted[25]. Here, we emphasize that a uniform polarization change through a non-polar high symmetry state is assumed for polarization switching, where formation of domains, effect of surface charges (depolarization field) in ultrathin films, and effect of electrodes are ignored for computational simplicity. These are also beyond the scope of this work. However, we compare our estimated switching barrier from uniform switching with that of known ferroelectrics to predict the possibility of realistic switching. Bennett *et al.* have proposed that switching barrier below 0.25 eV could be favorable for ferroelectric switching[58], and our value is lower than the proposed value. w-ScAlN can be a promising ferroelectric candidate as the switching barrier (0.16 eV/unit cell) is comparable with that of $PbTiO_3$ (0.20 eV/unit cell)[52], and lower than that of hexagonal ABC ferroelectrics[58]. Also note that ferroelectric polarization switching has been experimentally demonstrated in orthorhombic $GaFeO_3$ thin films, although there is a remarkably high energy barrier (1.05 eV per formula unit) for the switching[59].

To understand the origin of ferroelectricity, we compare the Born effective Charge (BEC) of the paraelectric (hexagonal) phase of AlN and the ScAlN superlattice. Our calculated Z^*_{33} for Al in h-AlN is 3.12 |e|, but is 3.35 |e| in h-ScAlN; Z^*_{33} of N is -3.12 |e| in h-AlN , but is -3.36 |e| (-3.81 |e|) for N bound to Al (N bound to Sc) in h-ScAlN ; Z^*_{33} of Sc in h-ScAlN is +3.82 |e|. Clearly, Z^*_{33} values in the paraelectric superlattice (h-ScAlN) are notably larger than the

formal charges of the elements, and also larger than the BECs in paraelectric h-AlN. Larger Z_{33}^* values compared to the formal charges indicate that the atomic displacements associated with the ferroelectric phase transition should be stemming from chemical activities, for example, charge transfer, intra-atomic redistribution of charge density, or rehybridization of covalent bonds. Indeed, a partial density of states (PDOS) analysis (Supplementary Information, Fig. S2 and Fig. S3) indicates that the phase transition from the hexagonal to the wurtzite is associated with a $3d_{z^2} - 3p_z$ hybridization at the Fermi level in the Sc atom (Fig. S2). This produces an asymmetric mixed orbital $\phi_{m(p_z)}$ along the z-direction, and causes an asymmetric Sc $\phi_{m(p_z)}$-N $2p_z$ hybridization (at the Fermi level) that results in an off-center displacement along the z-direction. $3d_{z^2} - 3s$ orbital mixing for Sc is present in h-ScAlN in the energy range of -4eV to -2eV (Supplementary Information, Fig. S3). However, this mixing produces a symmetric orbital $\phi_{m(s)}$, and therefore symmetric Sc$\phi_{m(s)}$-N $2p_z$ hybridization does not result in an off-center displacement. On the other hand, the Al-N layer undergoes sp^2-type to sp^3-type hybridization during the phase transition from the hexagonal to the wurtzite. Note that 'd^0-ness' (meaning empty d-states of ions like Ti^{4+} in BaTiO$_3$) with hybridization also plays vital role in driving the ferroelectric transition in YMnO$_3$[60-64].

A large structural change is still required for the polarization switching. During the transition from wurtzite to the intermediate hexagonal phase required for ferroelectric switching, the necessary 6.3% increase in the in-plane lattice parameters and the 15.80% decrease in the c-direction are likely to cause the bulk crystal to crack. On the other hand, when the crystal structure is not allowed to change in-plane, the energy difference between the wurtzite and the hexagonal phases of the ScAlN superlattice, with wurtzite's in-plane lattice parameters, is 0.63 eV (obtained from NEB calculation as shown in Fig. 1(a)), which is too high for practical memory devices. To understand the origin of this, the phonon band structure for the paraelectric (hexagonal) phase is computed using the basal plane lattice parameters fixed at those of w-ScAlN and allowing the c lattice parameter to relax. The same imaginary mode is

present at the Γ point and this mode becomes even softer (i11.60 THz), indicating that the polar wurtzite structure becomes more energetically preferable with respect to the hexagonal phase, and in-plane lattice expansion during switching reduces the energy barrier for the polarization switching. Therefore, we suggest that an epitaxially biaxial tensile strained thin film forced to have the basal plane lattice parameters matched to the substrate by forming a coherent film-substrate interface, and free to relax only along the c-direction, can be ideal for realizing ferroelectric switching. Such epitaxial strain can additionally prevent the thin film (usually a few hundred nanometers thick) cracking during polarization switching.

The switching barrier can also be profoundly decreased by epitaxial tensile strain as shown in Fig. 2(a). In our ordered structure, we find that an epitaxial biaxal tensile strain plays the similar role as the doping concentration of Sc in w-AlN, in that both internal parameters increase to 0.5 with the tensile strain (shown in Fig. 2(b)), indicating that the tensile strain leads the structure close to the phase transition from the wurtzite to the hexagonal. The softening of A_1 phonon modes with epitaxial tensile strain (Fig. S5 in Supplementary Information) also indicates the same phase transition. Furthermore, the switching barrier can be dramatically reduced; for example, at 5% biaxial strain, the energy barrier is only 0.08 eV/unit cell, which is smaller than that of perovskite $PbTiO_3$ (about 0.2 eV/unit cell)[52]. It should be mentioned that epitaxial strain has been experimentally demonstrated as an effective approach to engineer ferroectricity in other non-ferroelectric materials[39–41,65].

Now we discuss the effect of epitaxial strain on the spontaneous polarization as it enhances the polarization substantially in $PbTiO_3$ and $BaTiO_3$; but the polarization in $LiNbO_3$ or $BiFeO_3$ remains almost unaffected[66]. We find that total polarization (P) in w-ScAlN changes significantly under epitaxial strain (shown in Fig. 3). First, the P along the c-direction for each epitaxial strain is directly calculated using Eq. (1). Based on linear relation between the total spontaneous polarization change and strain, the P under an epitaxial strain is also estimated in terms of piezoelectric constants of unstrained structure by the following expression:
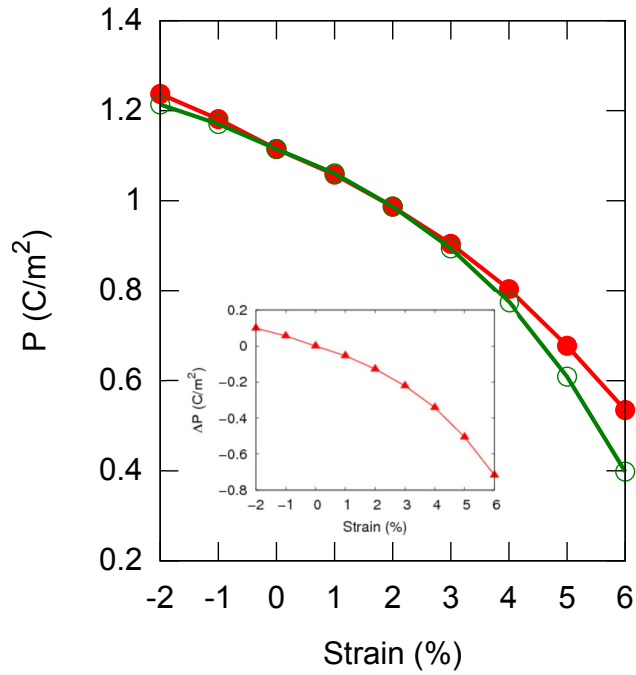
Figure 3: The total spontaneous polarization (P) along the c-direction as a function of epitaxial strain. Red filled circles represent directly calculated values using Eq. (1), and green open circles represent values estimated using Eq. (2). $\triangle P$, which is the change in spontaneous polarization along the c-direction due to the epitaxial strain, as a function of epitaxial strain is shown in the inset.

$$P = P_3 + \triangle P = P_3 + 2\epsilon(e_{31} - P_3) + \epsilon_3 e_{33} \tag{2}$$

Here, $\triangle P$ is the change in spontaneous polarization along the c-direction due to the epitaxial strain ϵ. Our calculated proper piezoelectric constant e_{31} (e_{33}) from DFPT calculations is -0.65 C/m^2 (1.79 C/m^2). ϵ_3 is the induced strain along the c-direction due to the in-plane epitaxial strain, which is calculated as the ratio between the change in the c lattice parameter due to the epitaxial strain to that of the unstrained structure. Fig. 3 shows the polarization obtained from both Eq. (1) and Eq. (2) as a function of epitaxial strain. In the range of strain -2% to 3%, polarizations obtained from both equations are very close, and the relation between strain and polarization is linear. We find that compressive (tensile) strain enhances (decreases) the P because of different sign of $\triangle P$ (shown in Fig 3). From structural point of view, compressive strain makes the ScN and AlN layers more buckled, hence increases the total P. On the other hand, tensile strain leads the polar wurtzite to the nonpolar hexagonal structure flatting the atomic layers, which consequently decreases the total P.

For practical device applications such as resonators, the out of plane piezoelectric constants determine device performance. The piezoelectric response of the w-ScAlN superlattice is calculated to be e_{33} = 1.78C/m^2(Table 1). This is larger than that of pure w-AlN (1.46C/m^2). Although disordered Sc-doped AlN has a much larger piezoelectric constant of 3.1 C/m^2 , that result is achieved for high Sc doping levels ($\approx$50%)[14], which induce the phase transition to the hexagonal structure that completely removes the piezoelectric effect.

To understand the origin of large piezoelectric constant in w-ScAlN, we decompose e_{33} into two contributions[67]:

$$e_{33} = e_{33}^{clamp} + \sum_k e_{33}^{int}(k) = e_{33}^{clamp} + \sum_k \frac{2e}{\sqrt{3}a^2} Z_{33}^*(k) \frac{du_3(k)}{d\eta_3} \tag{3}$$

The clamped-ion term (e_{33}^{clamp}) arises from the contributions of electrons when the ions
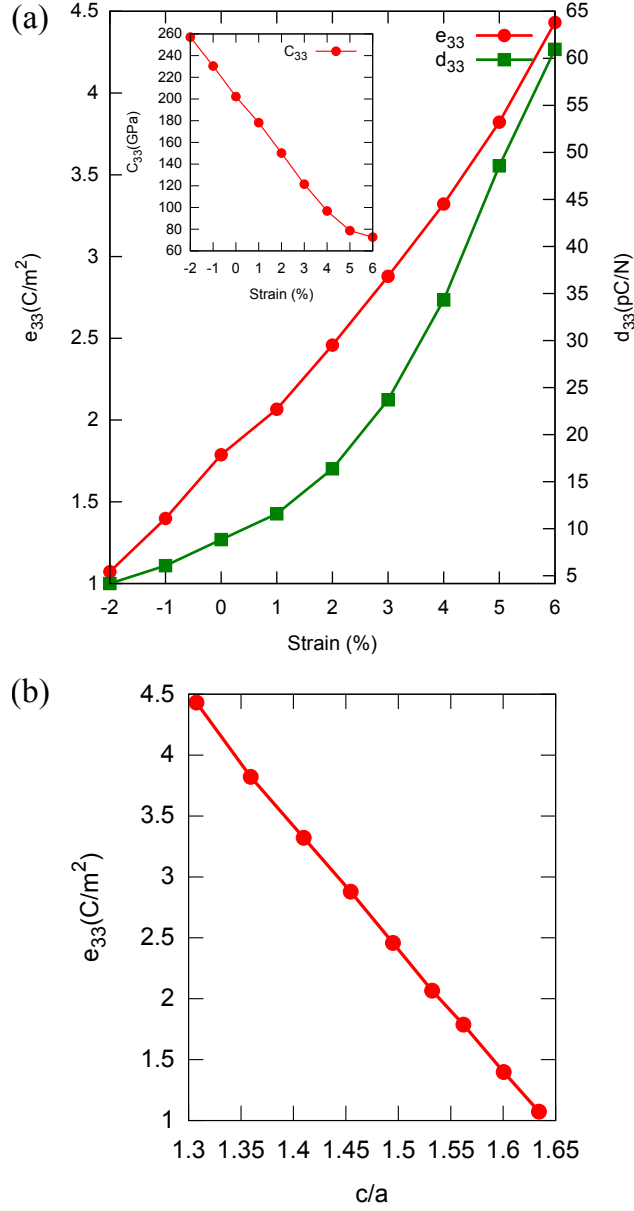
Figure 4: (a) Change in piezoelectric constants (e_{33} and d_{33}) with epitaxial strain. Inset shows the change in elastic constant C_{33} with epitaxial strain. (b) e_{33} as a function of the c/a ratio as the c/a ratio changes due to the epitaxial strain.

are frozen at their zero-strain equilibrium internal atomic coordinates (u); and the internal-strain (e_{33}^{int}) term arises from the contribution from internal microscopic atomic displacements in response to a macroscopic strain. In our case, the strain (η_3) is applied in the z-direction. Here, k runs over all the atoms in the unit cell, a is the in-plane lattice constant, and e is the electron charge. The Born effective charge ($Z_{33}^*(k)$) of k-th atom is calculated by the DFPT approach. The response of the k-th atom's internal coordinate along the c-direction ($u_3\ (k)$) to a macroscopic strain (η_3) is measured by $\frac{du_3(k)}{d\eta_3}$. From Table 1, it is clear that both BEC and internal-response for each atom in w-ScAlN are larger than those in w-AlN. Therefore, e_{33} is enhanced for the w-ScAlN superlattice compared to w-AlN. Note that the value of e_{33}^{int} for w-ScAlN (2.37 C/m^2) is significantly larger than for w-AlN (1.88 C/m^2), although the contribution from the electrons in w-ScAlN (-0.59 C/m^2) is only slightly larger than that in w-AlN (-0.42 C/m^2). Interestingly, we find that all the atoms contribute almost equally.

If we now consider epitaxial biaxal tensile strain, the BEC and the internal response term increase significantly. For example, at 5% strain, the internal-response term for each atom is almost doubled compared to that in w-ScAlN at zero strain. Additionally, e_{33}^{clamp} decreases with increasing strain, which also increases e_{33}. Therefore, we conclude that the larger e_{33} of the w-ScAlN superlattice under epitaxial strain (shown in Fig. 4(a)) primarily originates from the large increase in the BEC and the internal-response of atoms, where the electronic contribution also plays a role at large strain. Interestingly, we can also explain this increase of e_{33} in terms of the c/a ratio. Recently a linear relation between e_{33} and the c/a ratio has been proposed for various known wurtzite materials[68]. In Fig. 4(b), we see a similar linear relation between e_{33} and the c/a even for the w-ScAlN superlattice. The c/a ratio changes with epitaxial strain because the c lattice parameter decrease almost linearly with the tensile strain (as shown in Fig. 2(b)).

Using e_{33} and C_{33}, we estimate d_{33} as e_{33}/C_{33}[14]. Our calculated d_{33} of w-ScAlN (8.84 pC/N) is doubled compared to the value for w-AlN (4.08 pC/N). This is due to the significant increase in e_{33} and the decrease in C_{33} (358.34 GPa in w-AlN to 202.21 GPa in

Table 1: Born Effective Charges (Z_{33}^*) ($|e|$), $\frac{\partial u_3}{\partial \eta_3}$, $e_{33}^{int}(k)$ (C/m^2) , e_{33}^{int} (C/m^2), e_{33}^{clamp}(C/m^2) and total e_{33}(C/m^2).

Structure	Atom	Z_{33}^*	$\frac{\partial u_3}{\partial \eta_3}$	$e_{33}^{int}(k)$	e_{33}^{int}	e_{33}^{clamp}	e_{33}
w-AlN	Al	2.680	0.093	0.470	1.880	-0.423	1.457
	N	-2.678	-0.093	0.470			
w-ScAlN	Al	2.810	0.109	0.508	2.370	-0.586	1.784
	Sc	3.056	0.134	0.683			
	N_{Al}	-3.135	-0.114	0.592			
	N_{Sc}	-2.727	-0.130	0.587			
w-ScAlN (5%)	Al	2.938	0.229	1.013			
	Sc	3.252	0.202	0.992	3.995	-0.181	3.814
	N_{Al}	-3.344	-0.187	0.942			
	N_{Sc}	-2.844	-0.244	1.048			

w-ScAlN). As mentioned above, epitaxial biaxal tensile strain significantly enhances e_{33}, and it also profoundly softens C_{33} (shown in Fig. 4(a)). Consequently, we predict a significant enhancement in d_{33} with applied biaxial strain. For example, at a moderate 4% strain, d_{33} becomes about 35 pC/N, which is significantly larger than the highest d_{33} reported for unstable Sc-doped w-AlN[9].

Two interesting points should be mentioned. Firstly, only C_{33} is linearly decreasing with strain, as the other elastic coefficients remain essentially unaffected. This suggests a controlled approach to tune both the elastic and piezoelectric properties along only the c-direction while keeping the sample unaffected in-plane, which is of great benefit for device design. Secondly, as a consequence of the first point, the elastic stability criteria [$2C_{13}^2<$ $C_{33}(C_{11}+C_{12})$][49] no longer holds at 5% or larger strain, although the dynamical stability criterion (no imaginary phonon mode for all wave vectors) is still valid at 5% strain (Supplementary Information, Fig. S5). Therefore, we propose that the ideal epitaxial tensile strain will be in the range of 3-4%. Note that epitaxial strain engineering is a well-established technique for enhancing CMOS performance, engineering electronic bandstructure, searching for better catalysts, and improving ferroelectric, ferromagnetic, and superconducting transition temperatures[65,69–71]. Nowadays about $\pm 3\%$ epitaxial strains are common for oxide thin films; a strain as large as -6% has been demonstrated in BiFeO$_3$ thin films[69,72,73]. In this

regard, epitaxially grown nitrides are also quite common. For example, AlN and GaN have been grown on the Si(111) surface with large lattice mismatch[74,75]. Interestingly, strain has been even proposed to stabilize the structures for highly doped nitrides[25]. Suitable epitaxial strain can be induced by growing one nitride on another nitride substrate. For example, 660 nm thick InGaN ultrathin films have been grown on GaN[76]. Moreover, strain can be even tuned by doping the nitride substrate.

Conclusion

In conclusion, we show that a 1:1 w-ScAlN superlattice is dynamical as well as mechanically stable and possesses a ferroelectric spontaneous electric polarization. The barrier for ferroelectric switching can be significantly tuned with epitaxial tensile strain, indicating the possibility of ultrathin ferroelctric films. More importantly, the superlattice exhibits significantly larger piezoelectric response compared to pure w-AlN. The origin of large piezoelectric constant e_{33} is a combination of an enhancement in Born effective charges (Z_{33}) and the sensitivity of atomic co-ordinates with respect to external strain ($\frac{\partial u_3}{\partial \eta_3}$). In addition, the softening of the C_{33} elastic constant further promotes a larger d_{33}. We demonstrate that epitaxial biaxial tensile strain can significantly enhance the piezo-response. For example, d_{33} in w-ScAlN at 4% epitaxial tensile strain is about seven times larger than that of pure w-AlN. The applied tensile strain enhances e_{33} by increasing Z_{33} and $\frac{\partial u_3}{\partial \eta_3}$, together with a pronounced softening of C_{33}, which then significantly increases the value of d_{33}. As both superlattice growth and epitaxial strain have been previously experimentally demonstrated in wurtzite nitrides, our results can show a novel approach to add new functionalities such as ferroelectricity and tunable piezoelectrictricity to wurtzite nitrides.

Acknowledgement

References

(1) Moram, M. A.; Zhang, S. ScGaN and ScAlN: emerging nitride materials. *J. Mater. Chem. A* **2014**, *2*, 6042–6050.

(2) Sinha, N.; Wabiszewski, G. E.; Mahameed, R.; Felmetsger, V. V.; Tanner, S. M.; Carpick, R. W.; Piazza, G. Piezoelectric aluminum nitride nanoelectromechanical actuators. *Applied Physics Letters* **2009**, *95*, 053106.

(3) Karabalin, R. B.; Matheny, M. H.; Feng, X. L.; Defaÿ, E.; Le Rhun, G.; Marcoux, C.; Hentz, S.; Andreucci, P.; Roukes, M. L. Piezoelectric nanoelectromechanical resonators based on aluminum nitride thin films. *Applied Physics Letters* **2009**, *95*, 103111.

(4) Xiong, C.; Sun, X.; Fong, K. Y.; Tang, H. X. Integrated high frequency aluminum nitride optomechanical resonators. *Applied Physics Letters* **2012**, *100*, 171111.

(5) Piazza, G.; Felmetsger, V.; Muralt, P.; Olsson III, R. H.; Ruby, R. Piezoelectric aluminum nitride thin films for microelectromechanical systems. *MRS Bulletin* **2012**, *37*, 1051–1061.

(6) Rinaldi, M.; Zuniga, C.; Zuo, C.; Piazza, G. Super-high-frequency two-port AlN

contour-mode resonators for RF applications. *IEEE Transactions on Ultrasonics, Ferroelectrics, and Frequency Control* **2010**, *57*, 38–45.

(7) Muralt, P.; Antifakos, J.; Cantoni, M.; Lanz, R.; Martin, F. Is there a better material for thin film BAW applications than AlN? *IEEE Ultrasonics Symposium* **2005**, *1*, 315–320.

(8) Loebl, H.; Klee, M.; Metzmacher, C.; Brand, W.; Milsom, R.; Lok, P. Piezoelectric thin AlN films for bulk acoustic wave (BAW) resonators. *Materials Chemistry and Physics* **2003**, *79*, 143 – 146.

(9) Akiyama, M.; Kamohara, T.; Kano, K.; Teshigahara, A.; Takeuchi, Y.; Kawahara, N. Enhancement of Piezoelectric Response in Scandium Aluminum Nitride Alloy Thin Films Prepared by Dual Reactive Cosputtering. *Advanced Materials* **2009**, *21*, 593–596.

(10) Tholander, C.; Tasnádi, F.; Abrikosov, I. A.; Hultman, L.; Birch, J.; Alling, B. Large piezoelectric response of quarternary wurtzite nitride alloys and its physical origin from first principles. *Phys. Rev. B* **2015**, *92*, 174119.

(11) Uehara, M.; Shigemoto, H.; Fujio, Y.; Nagase, T.; Aida, Y.; Umeda, K.; Akiyama, M. Giant increase in piezoelectric coefficient of AlN by Mg-Nb simultaneous addition and multiple chemical states of Nb. *Applied Physics Letters* **2017**, *111*, 112901.

(12) Schneider, M.; DeMiguel-Ramos, M.; Flewitt, A. J.; Iborra, E.; Schmid, U. Scandium Aluminium Nitride-Based Film Bulk Acoustic Resonators. *Proceedings* **2017**, *1*, 305.

(13) Talley, K. R.; Millican, S. L.; Mangum, J.; Siol, S.; Musgrave, C. B.; Gorman, B.; Holder, A. M.; Zakutayev, A.; Brennecka, G. L. Implications of heterostructural alloying for enhanced piezoelectric performance of (Al,Sc)N. *Phys. Rev. Materials* **2018**, *2*, 063802.

(14) Tasnádi, F.; Alling, B.; Höglund, C.; Wingqvist, G.; Birch, J.; Hultman, L.; Abrikosov, I. A. Origin of the Anomalous Piezoelectric Response in Wurtzite $Sc_xAl_{1-x}N$ Alloys. *Phys. Rev. Lett.* **2010**, *104*, 137601.

(15) Tholander, C.; Abrikosov, I. A.; Hultman, L.; Tasnádi, F. Volume matching condition to establish the enhanced piezoelectricity in ternary $(Sc,Y)_{0.5}(Al,Ga,In)_{0.5}N$ alloys. *Phys. Rev. B* **2013**, *87*, 094107.

(16) Momida, H.; Teshigahara, A.; Oguchi, T. Strong enhancement of piezoelectric constants in $Sc_xAl1 - xN$: First-principles calculations. *AIP Advances* **2016**, *6*, 065006.

(17) Y Woo, S.; Bugnet, M.; P T Nguyen, H.; Zhao, S.; Mi, Z.; Botton, G. A. *European Microscopy Congress 2016: Proceedings*; American Cancer Society, pp 550–551.

(18) Ruterana, P.; Nouet, G.; Van der Stricht, W.; Moerman, I.; Considine, L. Chemical ordering in wurtzite $InxGa1 - xN$ layers grown on (0001) sapphire by metalorganic vapor phase epitaxy. *Applied Physics Letters* **1998**, *72*, 1742–1744.

(19) Ranjan, V.; Bin-Omran, S.; Sichuga, D.; Nichols, R. S.; Bellaiche, L.; Alsaad, A. Properties of GaN/ScN and InN/ScN superlattices from first principles. *Phys. Rev. B* **2005**, *72*, 085315.

(20) Ranjan, V.; Bin-Omran, S.; Bellaiche, L.; Alsaad, A. Isostructural phase transitions in GaN/ScN and InN/ScN superlattices. *Phys. Rev. B* **2005**, *71*, 195302.

(21) Wei, S.; Chee-Keong, T.; Nelson, T. III-Nitride Digital Alloy: Electronics and Optoelectronics Properties of the InN/GaN Ultra-Short Period Superlattice Nanostructures. *Scientific Reports* **2017**, *7*, 6671.

(22) Staszczak, G.; Gorczyca, I.; Grzanka, E.; Smalc-Koziorowska, J.; Targowski, G.; Czernecki, R.; Siekacz, M.; Grzanka, S.; Skierbiszewski, C.; Schulz, T.; Christensen, N. E.;

Suski, T. Bandgap behavior of InGaN/GaN short period superlattices grown by metal-organic vapor phase epitaxy. *physica status solidi (b)* **2017**, *254*, 1600710.

(23) Miao, Z. L.; Yu, T. J.; Xu, F. J.; Song, J.; Lu, L.; Huang, C. C.; Yang, Z. J.; Wang, X. Q.; Zhang, G. Y.; Zhang, X. P.; Yu, D. P.; Shen, B. Strain effects on InxAl1-xN crystalline quality grown on GaN templates by metalorganic chemical vapor deposition. *Journal of Applied Physics* **2010**, *107*, 043515.

(24) Lymperakis, L.; Schulz, T.; Freysoldt, C.; Anikeeva, M.; Chen, Z.; Zheng, X.; Shen, B.; Chèze, C.; Siekacz, M.; Wang, X. Q.; Albrecht, M.; Neugebauer, J. Elastically frustrated rehybridization: Origin of chemical order and compositional limits in InGaN quantum wells. *Phys. Rev. Materials* **2018**, *2*, 011601.

(25) Zhang, S.; Holec, D.; Fu, W. Y.; Humphreys, C. J.; Moram, M. A. Tunable optoelec-tronic and ferroelectric properties in Sc-based III-nitrides. *Journal of Applied Physics* **2013**, *114*, 133510.

(26) Yoshikawa, A.; Che, S. B.; Yamaguchi, W.; Saito, H.; Wang, X. Q.; Ishitani, Y.; Hwang, E. S. Proposal and achievement of novel structure InNâGaN multiple quantum wells consisting of 1 ML and fractional monolayer InN wells inserted in GaN matrix. *Applied Physics Letters* **2007**, *90*, 073101.

(27) Yoshikawa, A.; Kusakabe, K.; Hashimoto, N.; Hwang, E.-S.; Itoi, T. Dynamic atomic layer epitaxy of InN on/in +c-GaN matrix: Effect of âIn+Nâ coverage and capping timing by GaN layer on effective InN thickness. *Applied Physics Letters* **2016**, *108*, 022108.

(28) Kusakabe, K.; Hashimoto, N.; Itoi, T.; Wang, K.; Imai, D.; Yoshikawa, A. Growth kinetics and structural perfection of (InN)1/(GaN)1-20 short-period superlattices on +c-GaN template in dynamic atomic layer epitaxy. *Applied Physics Letters* **2016**, *108*, 152107.

(29) Islam, S. M.; Lee, K.; Verma, J.; Protasenko, V.; Rouvimov, S.; Bharadwaj, S.; (Grace) Xing, H.; Jena, D. MBE-grown 232-270 nm deep-UV LEDs using monolayer thin binary GaN/AlN quantum heterostructures. *Applied Physics Letters* **2017**, *110*, 041108.

(30) Gao, N.; Lin, W.; Chen, X.; Huang, K.; Li, S.; Li, J.; Chen, H.; Yang, X.; Ji, L.; Yu, E. T.; Kang, J. Quantum state engineering with ultra-short-period (AlN)m/(GaN)n superlattices for narrowband deep-ultraviolet detection. *Nanoscale* **2014**, *6*, 14733–14739.

(31) Woo, S. Y.; Bugnet, M.; Nguyen, H. P. T.; Mi, Z.; Botton, G. A. Atomic Ordering in InGaN Alloys within Nanowire Heterostructures. *Nano Letters* **2015**, *15*, 6413–6418.

(32) Little, M. E.; Kordesch, M. E. Band-gap engineering in sputter-deposited $Sc_xGa1-xN$. *Applied Physics Letters* **2001**, *78*, 2891–2892.

(33) Iliopoulos, E.; Ludwig, K. F.; Moustakas, T. D.; Chu, S. N. G. Chemical ordering in AlGaN alloys grown by molecular beam epitaxy. *Applied Physics Letters* **2001**, *78*, 463–465.

(34) Pakuła, K.; Borysiuk, J.; Boek, R.; Baranowski, J. Long-range order spontaneous superlattice in AlGaN epilayers. *Journal of Crystal Growth* **2006**, *296*, 191 – 196.

(35) Wu, Z. H.; Kawai, Y.; Fang, Y.-Y.; Chen, C. Q.; Kondo, H.; Hori, M.; Honda, Y.; Yamaguchi, M.; Amano, H. Spontaneous formation of highly regular superlattice structure in InGaN epilayers grown by molecular beam epitaxy. *Applied Physics Letters* **2011**, *98*, 141905.

(36) Daoust, P.; Desjardins, P.; Masut, R. A.; Gosselin, V.; Côté, M. Ab initio piezoelectric properties of $Al_{0.5}Sc_{0.5}N$: Impact of alloy configuration on the $d_{33,f}$ piezoelectric strain coefficient. *Phys. Rev. Materials* **2017**, *1*, 055402.

(37) Budimir, M.; Damjanovic, D.; Setter, N. Enhancement of the piezoelectric response of tetragonal perovskite single crystals by uniaxial stress applied along the polar axis: A free-energy approach. *Phys. Rev. B* **2005**, *72*, 064107.

(38) Wu, Z.; Cohen, R. E. Pressure-Induced Anomalous Phase Transitions and Colossal Enhancement of Piezoelectricity in $PbTiO_3$. *Phys. Rev. Lett.* **2005**, *95*, 037601.

(39) Zhang, Y.; Wang, J.; Sahoo, M. P. K.; Shimada, T.; Kitamura, T. Strain-induced ferroelectricity and lattice coupling in BaSnO3 and SrSnO3. *Phys. Chem. Chem. Phys.* **2017**, *19*, 26047–26055.

(40) Zhang, Y.; Sahoo, M. P. K.; Shimada, T.; Kitamura, T.; Wang, J. Strain-induced improper ferroelectricity in Ruddlesden-Popper perovskite halides. *Phys. Rev. B* **2017**, *96*, 144110.

(41) Bousquet, E.; Spaldin, N. A.; Ghosez, P. Strain-Induced Ferroelectricity in Simple Rocksalt Binary Oxides. *Phys. Rev. Lett.* **2010**, *104*, 037601.

(42) Perdew, J. P.; Burke, K.; Ernzerhof, M. Generalized Gradient Approximation Made Simple. *Phys. Rev. Lett.* **1996**, *77*, 3865.

(43) Kresse, G.; Furthmüller, J. Efficient iterative schemes for ab initio total-energy calculations using a plane-wave basis set. *Phys. Rev. B* **1996**, *54*, 11169.

(44) Kresse, G.; Joubert, D. From ultrasoft pseudopotentials to the projector augmented-wave method. *Phys. Rev. B* **1999**, *59*, 1758.

(45) Togo, A.; Tanaka, I. First principles phonon calculations in materials science. *Scr. Mater.* **2015**, *108*, 1–5.

(46) Henkelman, G.; Uberuaga, B. P.; Jónsson, H. A climbing image nudged elastic band method for finding saddle points and minimum energy paths. *The Journal of Chemical Physics* **2000**, *113*, 9901–9904.

(47) Sheppard, D.; Xiao, P.; Chemelewski, W.; Johnson, D. D.; Henkelman, G. A generalized solid-state nudged elastic band method. *The Journal of Chemical Physics* **2012**, *136*, 074103.

(48) Zoroddu, A.; Bernardini, F.; Ruggerone, P.; Fiorentini, V. First-principles prediction of structure, energetics, formation enthalpy, elastic constants, polarization, and piezo-electric constants of AlN, GaN, and InN: Comparison of local and gradient-corrected density-functional theory. *Phys. Rev. B* **2001**, *64*, 045208.

(49) Mouhat, F.; Coudert, F.-X. Necessary and sufficient elastic stability conditions in various crystal systems. *Phys. Rev. B* **2014**, *90*, 224104.

(50) Dreyer, C. E.; Janotti, A.; Van de Walle, C. G.; Vanderbilt, D. Correct Implementation of Polarization Constants in Wurtzite Materials and Impact on III-Nitrides. *Phys. Rev. X* **2016**, *6*, 021038.

(51) Ghosez, P.; Michenaud, J.-P.; Gonze, X. Dynamical atomic charges: The case of ABO_3 compounds. *Phys. Rev. B* **1998**, *58*, 6224–6240.

(52) Simuck, F.; Krishna Chaitanya, P.; Serge M., N.; Markus, E.; Ying Wai, L.; Valentino R., C. Towards an accurate description of perovskite ferroelectrics: exchange and correlation effects. *Scientific Reports* **2017**, *7*, 43482.

(53) Tuttle, B.; Payne, D.; Mukherjee, J. Spontaneous Polarization for Ferroelectric Materials. *MRS Bulletin* **1994**, *19*, 20â20.

(54) Farrer, N.; Bellaiche, L. Properties of hexagonal ScN versus wurtzite GaN and InN. *Phys. Rev. B* **2002**, *66*, 201203.

(55) Takeuchi, N. First-principles calculations of the ground-state properties and stability of ScN. *Phys. Rev. B* **2002**, *65*, 045204.

(56) Constantin, C.; Haider, M. B.; Ingram, D.; Smith, A. R.; Sandler, N.; Sun, K.; Orde-jón, P. Composition-dependent structural properties in ScGaN alloy films: A combined experimental and theoretical study. *Journal of Applied Physics* **2005**, *98*, 123501.

(57) Constantin, C.; Al-Brithen, H.; Haider, M. B.; Ingram, D.; Smith, A. R. ScGaN alloy growth by molecular beam epitaxy: Evidence for a metastable layered hexagonal phase. *Phys. Rev. B* **2004**, *70*, 193309.

(58) Bennett, J. W.; Garrity, K. F.; Rabe, K. M.; Vanderbilt, D. Hexagonal *ABC* Semiconductors as Ferroelectrics. *Phys. Rev. Lett.* **2012**, *109*, 167602.

(59) Song, S.; Jang, H. M.; Lee, N.-S.; Son, J. Y.; Gupta, R.; Garg, A.; Ratanapreechachai, J.; Scott, J. F. Ferroelectric polarization switching with a remarkably high activation energy in orthorhombic GaFeO3 thin films. *Npg Asia Materials* **2016**, *8*, e242.

(60) Oak, M.-A.; Lee, J.-H.; Jang, H. M. Asymmetric Ho 5d-O 2p hybridization as the origin of hexagonal ferroelectricity in multiferroic $HoMnO_3$. *Phys. Rev. B* **2011**, *84*, 153106.

(61) Kim, J.; Cho, K. C.; Koo, Y. M.; Hong, K. P.; Shin, N. Y-O hybridization in the ferroelectric transition of YMnO3. *Applied Physics Letters* **2009**, *95*, 132901.

(62) Zhong, C.; Jiang, Q.; Zhang, H.; Jiang, X. Effect of spin frustration and spin-orbit coupling on the ferroelectric polarization in multiferroic YMnO3. *Applied Physics Letters* **2009**, *94*, 224107.

(63) Oak, M.-A.; Lee, J.-H.; Jang, H. M.; Goh, J. S.; Choi, H. J.; Scott, J. F. 4d−5p Orbital Mixing and Asymmetric In 4d − O 2p Hybridization in $InMnO_3$: A New Bonding Mechanism for Hexagonal Ferroelectricity. *Phys. Rev. Lett.* **2011**, *106*, 047601.

(64) Song, S.; Kim, D.; Jang, H. M.; Yeo, B. C.; Han, S. S.; Kim, C. S.; Scott, J. F.

β -CuGaO2 as a Strong Candidate Material for Efficient Ferroelectric Photovoltaics. *Chemistry of Materials* **2017**, *29*, 7596–7603.

(65) Lu, X.-Z.; Rondinelli, J. M. Epitaxial-strain-induced polar-to-nonpolar transitions in layered oxides. *Nature Materials* **2016**, *15*, 951–955.

(66) Ederer, C.; Spaldin, N. A. Effect of Epitaxial Strain on the Spontaneous Polarization of Thin Film Ferroelectrics. *Phys. Rev. Lett.* **2005**, *95*, 257601.

(67) Bernardini, F.; Fiorentini, V.; Vanderbilt, D. Spontaneous polarization and piezoelectric constants of $III - V$ nitrides. *Phys. Rev. B* **1997**, *56*, R10024–R10027.

(68) Momida, H.; Oguchi, T. Effects of lattice parameters on piezoelectric constants in wurtzite materials: A theoretical study using first-principles and statistical-learning methods. *Applied Physics Express* **2018**, *11*, 041201.

(69) Schlom, D. G.; Chen, L.-Q.; Fennie, C. J.; Gopalan, V.; Muller, D. A.; Pan, X.; Ramesh, R.; Uecker, R. Elastic strain engineering of ferroic oxides. *MRS Bulletin* **2014**, *39*, 118–130.

(70) Bedell, S.; Khakifirooz, A.; Sadana, D. Strain scaling for CMOS. *MRS Bulletin* **2014**, *39*, 131–137.

(71) Yildiz, B. Stretching the energy landscape of oxides-Effects on electrocatalysis and diffusion. *MRS Bulletin* **2014**, *39*, 147–156.

(72) Martin, L. W.; Schlom, D. G. Advanced synthesis techniques and routes to new single-phase multiferroics. *Current Opinion in Solid State and Materials Science* **2012**, *16*, 199 – 215.

(73) Christen, H. M.; Nam, J. H.; Kim, H. S.; Hatt, A. J.; Spaldin, N. A. Stress-induced $R - M_A - M_C - T$ symmetry changes in $BiFeO_3$ films. *Phys. Rev. B* **2011**, *83*, 144107.

(74) Tamariz, S.; Martin, D.; Grandjean, N. AlN grown on Si(111) by ammonia-molecular beam epitaxy in the 900-1200 °C temperature range. *Journal of Crystal Growth* **2017**, *476*, 58 – 63.

(75) Louarn, A. L.; Vézian, S.; Semond, F.; Massies, J. AlN buffer layer growth for GaN epitaxy on (111) Si: Al or N first? *Journal of Crystal Growth* **2009**, *311*, 3278 – 3284.

(76) Rao, M.; Kim, D.; Mahajan, S. Compositional dependence of phase separation in InGaN layers. *Applied Physics Letters* **2004**, *85*, 1961–1963.